Observation of magnetic vortex pairs at room temperature in a planar α-Fe_2O_3/Co heterostructure.

F. P. Chmiel,[1] N. Waterfield Price,[1] R. D. Johnson,[1] A. D. Lamirand,[2] J. Schad,[3] G. van der Laan,[2] D. T. Harris,[3] J. Irwin,[4] M. S. Rzchowski,[4] C.-B. Eom,[3] and P. G. Radaelli[1]

[1]*Clarendon Laboratory, Department of Physics, University of Oxford, Parks Road, Oxford OX1 3PU, United Kingdom*

[2]*Diamond Light Source, Harwell Science and Innovation Campus, Didcot OX11 0DE, United Kingdom*

[3]*Department of Materials Science and Engineering, University of Wisconsin-Madison, Madison, Wisconsin 53706, USA*

[4]*Department of Physics, University of Wisconsin-Madison, Madison, Wisconsin 53706, USA*

Abstract

Vortices, occurring whenever a flow field 'whirls' around a one-dimensional core, are among the simplest topological structures, ubiquitous to many branches of physics. In the crystalline state, vortex formation is rare, since it is generally hampered by long-range interactions: in ferroic materials (ferromagnetic and ferroelectric), vortices are only observed when the effects of the dipole-dipole interaction is modified by confinement at the nanoscale,[1–3] or when the parameter associated with the vorticity does not couple directly with strain.[4] Here, we observe an unprecedented form of vortices in antiferromagnetic (AFM) hematite (α-Fe_2O_3) epitaxial films, in which the primary whirling parameter is the staggered magnetisation. Remarkably, ferromagnetic (FM) topological objects with the same vorticity and winding number as the α-Fe_2O_3 vortices are imprinted onto an ultra-thin Co ferromagnetic over-layer by interfacial exchange. Our data suggest that the ferromagnetic vortices may be merons (half-skyrmions, carrying an out-of plane core magnetisation), and indicate that the vortex/meron pairs can be manipulated by the application of an in-plane magnetic field, giving rise to large-scale vortex-antivortex annihilation.

α-Fe_2O_3 is a 'classic' room-temperature antiferromagnet, with a Néel temperature of 948 K and the trigonal corundum crystal structure (space group $R\bar{3}c$). The Fe moments lie in the basal *ab* plane and are antiferromagnetically ordered along *c* (Fig. 1). We grew 10 nm-thick α-Fe_2O_3 epitaxial films with a Co (1 nm) / Al (1 nm) overlayer on a (0001)-Al_2O_3 substrate by magnetron sputtering (see Methods). The Co layer was confirmed to be ferromagnetically ordered, with easy-plane anisotropy, by Magneto-Optical Kerr Effect magnetometry (MOKE, see Methods) and its coercive field was found to be ~ 8 mT. Vector-mapped x-ray magnetic linear (for α-Fe_2O_3) and circular (for Co) photoemission electron microscopy (XMLD-PEEM and XMCD-PEEM) dichroism images were collected at room temperature and zero applied magnetic field at the Fe-L_3 and Co- L_3 edges respectively, using the I06 beamline at the Diamond Light Source, Didcot, UK. Exploiting the anisotropy of the XMLD / XMCD signal, data collected at different sample rotations were combined, to determine absolutely the direction parallel/anti-parallel to the AFM spins and the Co spin direction at the same positions on the surface of the sample (Fig. 1).[5–8] We found that the α-Fe_2O_3 spins are perpendicular to both the crystallographic *c*-axis and to one of the three 2-fold axes (magnetic space group $C2/c$), as previously reported.[9, 10] The three possible orientations of the AFM moments, related by the broken 3-fold rotation axis of the crystallographic structure, form an intricate domain structure (Fig. 2 a) at the scale of a few tens of nm. One prominent feature of the domain structure is the presence of 'pinch-points' between α-Fe_2O_3 domains of the same orientation. Around these points, domains are typically arranged in a 6-sector pinwheel, colors alternating as either R-G-B-R-G-B or R-B-G-R-B-G clockwise around their common core (here, 'R' represents α-Fe_2O_3 domains with the AFM spin direction parallel to [2,1,0], 'B' to [1,2,0] and 'G' to [-2,1,0] in the hexagonal setting of the unit cell, see Fig. 1 c). Overall, the domain morphology is strikingly reminiscent both of the disclination domains in liquid crystals[11] and of the cloverleaf *ferroelectric* domain patterns imaged in the hexagonal manganite $YMnO_3$ by piezoelectric force microscopy (PFM), pointing towards a common phenomenology in completely different contexts.[4, 12] Remarkably, at the phenomenological level there is an almost complete analogy between AFM ordering in α-Fe_2O_3 and structural ordering in $YMnO_3$, so that the terms in the Landau free energy expansion that contain only the principal order parameter are exactly the same up to at least the sixth order (See Supplementary Information for further details).[13]

It is important to emphasise the crucial relationship between the phenomenological Landau free energy and the observation of topological structures such as vortices. This subject was thoroughly discussed in a famous 1976 paper by T. Kibble on cosmic strings formation in the early universe [14], but can be applied, with appropriate modifications, to many other branches of physics. In all previously known cases, vortex formation is associated with a phase transition between a phase that is *topologically trivial* (non-superconducting, non-superfluid, disordered liquid crystals, gauge-invariant vacuum etc.) and one that is topologically rich enough to support vortices (superconducting, superfluid, nematic or smectic liquid crystals, symmetry-broken vacuum etc.) Therefore, the phenomenological equivalence between $YMnO_3$ and α-Fe_2O_3 proves that the latter can support vortices in the antiferromagnetic phase, in spite of the differences between the two systems (for example, in the

case of α-Fe_2O_3, the order parameter is magnetic rather than structural). More broadly, the Landau free energies of both $YMnO_3$ and α-Fe_2O_3 approach the U(1) symmetry of the Kibble model in the limit of a small order parameter, which is one way of satisfying the criterion of sufficient topological richness (see Supplementary Information). This being the case, vortices *will form by statistical necessity* when crossing the phase transition as a function of temperature. At lower temperatures, new vortex/antivortex pairs may form or, conversely, existing vortex/antivortex pairs may annihilate, with the second process being dominant at lower temperatures. In the case of a thermal transition, the Kibble-Zurek model [15] predicts that the number of vortices/antivortices surviving at low temperatures depends on the quenching rate through the transition, and this relation is also observed in the hexagonal manganites.[16] Since our α-Fe_2O_3 films were grown far below the Nèel temperature, one would expect that a significant population of vortices and antivortices, both free and bound, will be frozen in at growth. One may also expect that AFM vortices will form in bulk α-Fe_2O_3 single crystals that are rapidly quenched through the Nèel transition.

On this basis, the Fe L_3 XMLD-PEEM images can be straightforwardly interpreted: the 'pinch-points' are the *loci* of 180° domain boundaries, where the AFM order parameter has the same orientation but changes sign across the pinched boundary. Such boundaries are unfavourable energetically and are reduced to points (lines parallel to the film normal in 3 dimensions) during the domain formation, whilst the most favourable 60° domain walls end up dominating. While the XMLD-PEEM method is insensitive to this change in sign of the AFM order parameter, the pinched domain structure allows us to conclude, in analogy to the hexagonal manganites,[4] that the 'pinwheels' we observe are AFM vortices (R-G*-B-R*-G-B*; winding number +1) and anti-vortices (R-B*-G-R*-B-G*; winding number -1), asterisks denoting time inversion. The vortices /anti-vortices form a relatively dense network, with approximately 40 instances over a 80 μm^2 area. There are several closely-bound vortex/antivortex pairs, as well as isolated vortices, suggesting that the sample has been quenched without undergoing a Kosterlitz-Thouless transition.[17] Thus far, AFM vortices had only been created in nanoscale disk heterostructures by imprinting from FM vortices,[18, 19] and have never been previously observed in a homogeneous system.

Co- L_3 XMCD-PEEM images (Fig. 2 b) revealed that the Co film, which at this thickness is magnetically very soft, was found to be strongly textured at the sub-micron scale. The Co spins tended to align strongly *parallel* to the α-Fe_2O_3 spin direction, so that the α-Fe_2O_3 and the Co vector maps share a similar morphology (Fig. 2 a and b). Strikingly, the topological features of the α-Fe_2O_3 magnetism are *also* imprinted on the Co over-layer. In particular, FM vortices and anti-vortices are clearly visible on top of corresponding α-Fe_2O_3 features with the *same* winding number (Fig. 2 a and b) with the vortex cores being precisely aligned within the resolution of our measurements. Figure 3 displays numerical differentiation of the XMCD-PEEM images, which enabled us to pinpoint exactly the location and nature of the FM vortices and antivortices: clock-wise and anticlock-wise vortices are most apparent in the maps of the curl of the Co magnetisation, while antivortices display an angular alternation of curl in different sectors. The typical vortex core size, extracted from the full width at half maximum of maps of the magnitude of the Co magnetisation (Fig. 3 c), is of the order of 100 nm and appears to be limited by the resolution of our experiment. Once again, we

emphasise that FM vortices were only previously observed in nanodots.[3, 20]
In magnetic vortex structures, even with strong planar-anisotropy, the magnetisation often points out-of-the plane at the vortex core to satisfy unfavourable exchange and dipole interactions.[21] Indeed, in our XMCD-PEEM images we observe a reduction of the magnitude of the XMCD, sensitive only to the in-plane magnetisation (Fig. 3 c), which is compatible with the presence of an out-of-plane component of the Co spins at the vortex core. This raises the intriguing possibility that the FM topological structures we observe are *merons/antimerons* (also known as half-skyrmions)[22] rather than planar vortices/antivortices (Fig. 3 a), imprinted by interfacial exchange with the adjacent AFM vortex/anti-vortex in the α-Fe_2O_3 film. To test the feasibility of this scenario we have performed a set of micromagnetic simulations (see Supplementary Information) where a fixed, discrete α-Fe_2O_3 vortex is adjacent to an initially randomized Co layer. We find that the Co layer relaxes into a vortex state with the same topology of the AFM. Notably, at the core of the FM vortex an out-of-plane moment forms, confirming that it is indeed possible to imprint FM merons from an adjacent AFM. Although the out-of-plane magnetic moment of the meron core is not a topological invariant, reversing it by a global rotation in spin space requires 'unwinding' the meron, which is strongly disfavoured by the easy-plane anisotropy, meaning the moment at the core should be stable to small external perturbation.
We found it is possible to manipulate the vortex/meron pairs by the application of moderate magnetic fields. To achieve this, we applied an *ex-situ* 100 mT field parallel to [1,1,0] and re-aligned the sample in the same position under the electron microscope. Figures 2 and 4 show the remarkable end result of this process: domains not involved in 'pinch-points' are largely invariant, (e.g., Fig. 4 c and d), meaning that the large-scale features of the vector map are mostly unchanged. However, large scale vortex/antivortex annihilation has clearly occurred, removing all 'pinch-points' from the α-Fe_2O_3 film, Fig. 4 a and b. This phenomenon is confirmed by the Co L_3 XMCD-PEEM vector map (Fig. 2 d) of the Co overlayer: although the Co spins maintain a strong tendency to align along the direction of the α-Fe_2O_3 staggered magnetisation, the vast majority of FM vortex/merons have disappeared. Our observation of a dense population of coupled AFM/FM vortex pairs in a planar homogeneous α-Fe_2O_3/Co heterostructure indicates multiple avenues for exploitation in both fundamental and applied research. At the fundamental level, this system represents a purely magnetic realisation of the Kibble-Zurek model with discrete Z_6 symmetry, which has been previously studied in as a structural realisation in $YMnO_3$.[23] The close proximity to room temperature of the first-order Morin transition ($\sim$ 260 K for bulk α-Fe_2O_3, tuneable by film thickness and doping),[24] below which the Fe spins flop along the c axis and all AFM vortices must disappear, provides a further opportunity to study the first-order analogue of the Kibble-Zurek model, in which the string density is controlled by nucleation rather than fluctuations. On the applied side, FM merons can be thought of as topologically protected spin 'bits', and could be very appealing for information storage in both pinned and free forms. A regular array of pinned merons, arranged for example in a cross-point architecture,[25] could store information in the magnetisaton of the FM meron core, in analogy to proposed memories based on arrays of FM nanodots.[26] If a population imbalance between merons and antimerons could be created, free merons could be produced by cooling

below the Morin transition. Such a hypothetical device could serve as a source for 'meron racetrack memories', similar to those currently considered for skyrmions.[27, 28]

Acknowledgements

We acknowledge Diamond Light Source for time on Beam Line I06 under Proposal SI16338 and SI15088. We thank S. Parameswaran for discussions and T. Hesjedal and S. Zhang for assistance with initial film growth. The work done at the University of Oxford (F. P. C, N. W. P., R. D. J., and P. G. R.) is funded by EPSRC Grant No. EP/M020517/1, entitled Oxford Quantum Materials Platform Grant. The work at University of Wisconsin-Madison (J.S., J. I., M. S. R. and C.-B. E.) supported by the Army Research Office through Grant No. W911NF-13-1-0486 and W911NF-17-1-0462. R. D. J. acknowledges support from a Royal Society University Research Fellowship.

Author Contributions

F. P. C., N. W. P., R. D. J. and A. D. L. performed the experiment. F. P. C. and A. D. L. performed the data reduction. F. P. C and N. W. P. performed the data analysis. J. S grew the films. D. T. H. made the α-Fe_2O_3 sputtering target. J. S and F. P. C. characterised the epitaxial relation of the films. J. I. performed the MOKE measurement. G. v. L. performed calculations of the XMLD signal. N. W. P. performed the micromagnetic simulations. P. G. R conceived and designed the experiment and supervised the analysis together with R. D. J, while C.-B. E. supervised the film growth. M. S. R. supervised the MOKE measurement. P. G. R. and F. P. C prepared the first draft of the manuscript. All authors discussed and contributed to the manuscript.

Competing Interests

The authors declare no competing interests.

Correspondence and request for materials

Correspondence should be addressed to P. G. R. or F. P. C and request for materials to C.-B. E. or J. S.

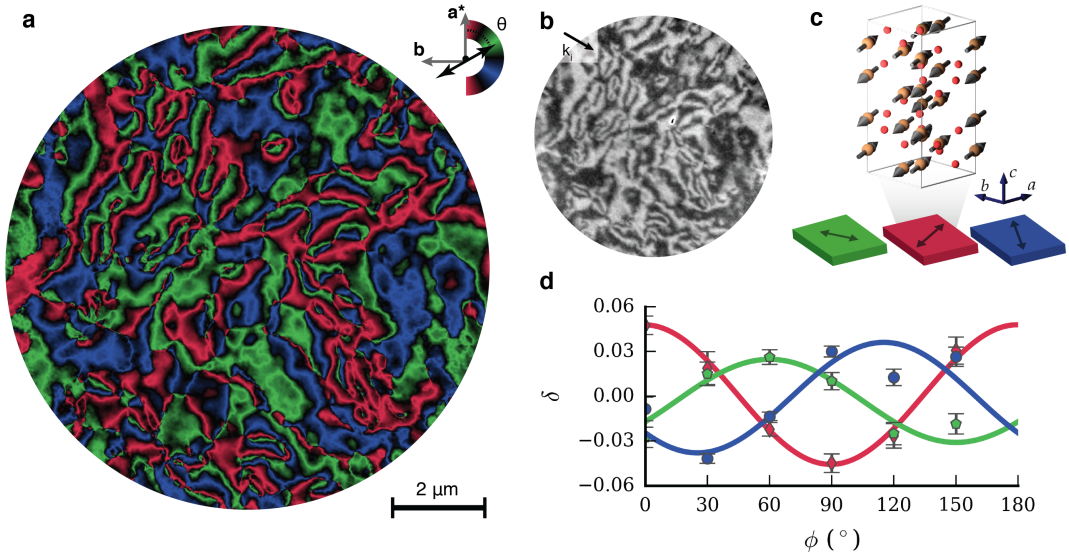

FIG. 1: Vector map of α-Fe_2O_3 antiferromagnetic domain configuration from x-ray photoemission microscopy. a, α-Fe_2O_3 domain structure constructed using the anisotropy of the XMLD signal. **b,** Measured XMLD signal for a single incident x-ray direction (azimuth), denoted by the solid black arrow. **c,** Graphic displaying the magnetic unit cell of α-Fe_2O_3 and the three antiferromagnetic orientation domains. **d,** Mean dichroism (XMLD signal), as a function of azimuth, for three 15 x 15 pixel regions, one in each of the three identified domains. Solid lines are the fits assuming a single AFM spin direction in each region.

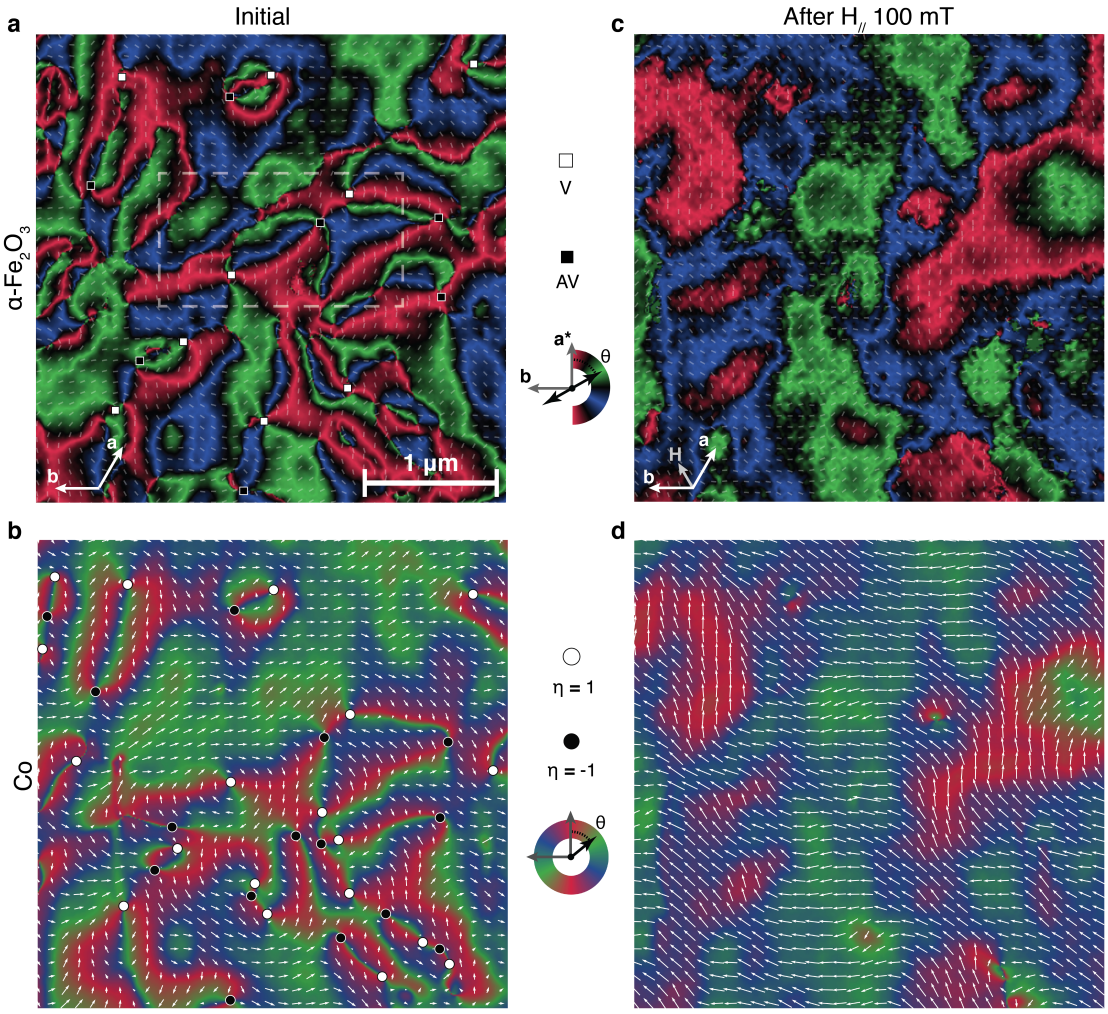

FIG. 2: Magnetic domain structure of α-Fe_2O_3 / Co film. a, Initial α-Fe_2O_3 antiferromagnetic domain structure as determined by vector - mapped XMLD-PEEM. White (black) squares indicate the approximate centre of identified vortex (anti-vortex) cores. White bars display the measured antiferromagnetic spin direction for a ten square pixel region; color represents the angle of the antiferromagnetic spin direction for each pixel measured clockwise from a*. Black regions highlight AFM spin directions deviating significantly from the three expected AFM spin directions of α-Fe_2O_3, primarily highlighting resolution-limited domain walls. The dashed white box shows the region of interest used in Fig. 3. **b,** Co spin vector map determined from XMCD-PEEM, white (black) circles are topological defects with a winding number of 1 (-1), see Methods for details. White arrows show the local in-plane spin orientation of the Co film for a ten square pixel region and color the angle of the spin, for each pixel, measured clockwise from a*. **c-d,** α-Fe_2O_3 and Co vector map after application of an *ex-situ*, 100 mT magnetic field along [1,1,0]. All images were recorded at the same position on the sample surface.

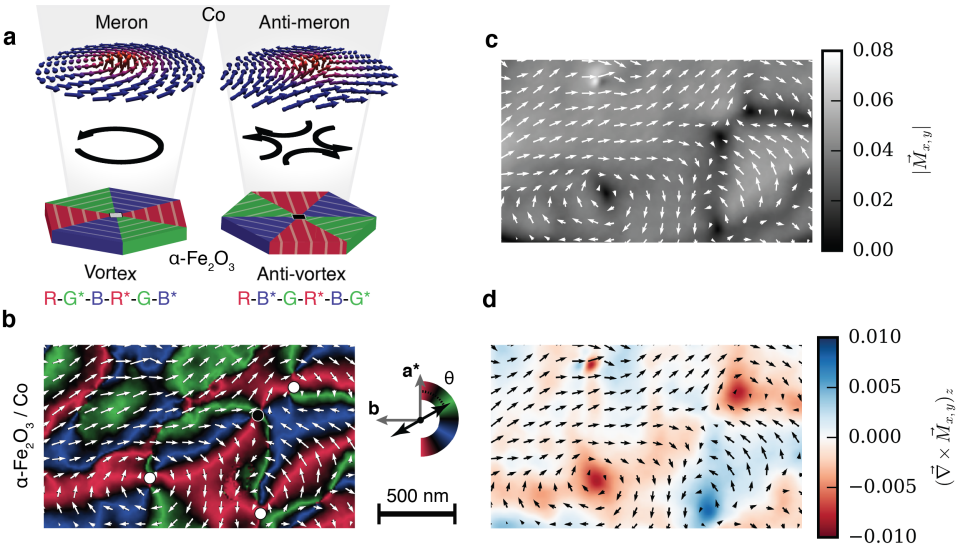

FIG. 3: Topological defects in α-Fe_2O_3 and Co. a, Graphic demonstrating coupling between α-Fe_2O_3 (anti-)vortices and Co (anti-)merons. **b,** Combined ferromagnetic (white arrows) and antiferromagnetic (colour) α-Fe_2O_3 / Co film domain structure for a small area of our film, shown by the dashed box in Fig. 2 a. White (black) circles show topological defects with a winding number of +1(-1). **c** Measured magnitude of Co magnetisation in the sample plane. The intensity reduction at the vortex cores is compatible with the meron picture (see text), although resolution smearing could produce similar effects. **d,** $\hat{z}$ component of the curl of the Co vector map.

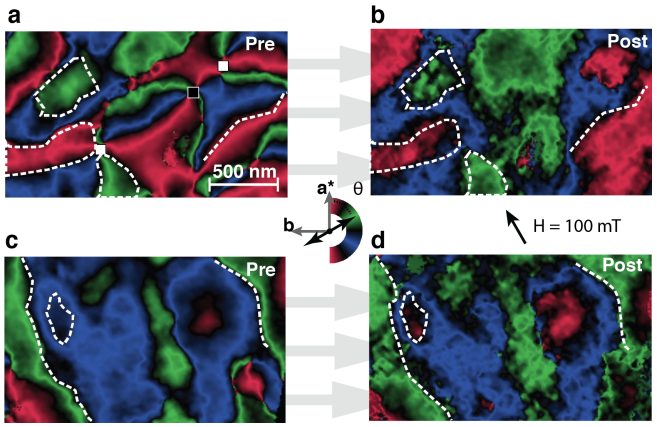

FIG. 4: Vortex annihilation with *ex-situ* applied field. a-d, Measured α-Fe_2O_3 domain configuration in two different regions of the sample before, a and c, and after, b and d, application of the 100 mT in-plane ([1,1,0]) magnetic field. The Co spins share a similar evolution see Fig. 2 b and d.

[1] Zheng, Y. & Chen, W. Characteristics and controllability of vortices in ferromagnetics, ferroelectrics and multiferroics. *Rep. Prog. Phys.* **80**, 086501 (2017).

[2] Yadav, A. K. *et al.* Observation of polar vortices in oxide superlattices. *Nature* **530**, 198–201 (2016).

[3] Cowburn, R. P., Koltsov, D. K., Adeyeye, A. O., Welland, M. E. & Tricker, D. M. Single-domain circular nanomagnets. *Phys. Rev. Lett.* **83**, 1042 (1999).

[4] Choi, T. *et al.* Insulating interlocked ferroelectric and structural antiphase domain walls in multiferroic $YMnO_3$. *Nat. Mater.* **9**, 253 (2010).

[5] Hallsteinsen, I. *et al.* Magnetic domain configuration of (111)-oriented $LaFeO_3$ epitaxial thin films. *Appl. Phys. Lett. Mater.* **5**, 086107 (2017).

[6] Waterfield Price, N. *et al.* Coherent magnetoelastic domains in multiferroic $BiFeO_3$ films. *Phys. Rev. Lett.* **117**, 177601 (2016).

[7] Alders, D. *et al.* Magnetic x-ray dichroism study of the nearest-neighbor spin-spin correlation function and long-range magnetic order parameter in antiferromagnetic NiO. *Europhys. Lett.* **32**, 259 (1995).

[8] Scholl, A., Ohldag, H., Nolting, F., Stöhr, J. & Padmore, H. A. X-ray photoemission electron microscopy, a tool for the investigation of complex magnetic structures. *Rev. Sci. Instrum.* **73**, 1362–1366 (2002).

[9] Chen, P., Lee, N., McGill, S., Cheong, S.-W. & Musfeldt, J. Magnetic-field-induced color change in α-Fe_2O_3 single crystals. *Phys. Rev. B* **85**, 174413 (2012).

[10] Marmeggi, J. C., Hohlwein, D. & Bertaut, E. F. Magnetic neutron Laue diffraction study of the domain distribution in α-Fe_2O_3. *Phys. Stat. Sol. (a)* **39**, 57–64 (1977).

[11] Nehring, J. & Saupe, A. On the schlieren texture in nematic and smectic liquid crystals. *J. Chem. Soc., Faraday Trans. 2* **68**, 1 (1972).

[12] Chae, S. C. *et al.* Direct observation of the proliferation of ferroelectric loop domains and vortex-antivortex pairs. *Phys. Rev. Lett.* **108**, 167603 (2012).

[13] Artyukhin, S., Delaney, K. T., Spaldin, N. A. & Mostovoy, M. Landau theory of topological defects in multiferroic hexagonal manganites. *Nat. Mater.* **13**, 42–49 (2013).

[14] Kibble, T. W. B. Topology of cosmic domains and strings. *J. Phys. A: Math. Gen.* **9**, 1387–1398 (1976).

[15] Zurek, W. H. Cosmological experiments in superfluid helium? *Nature* **317**, 505–508 (1985).

[16] Meier, Q. N. *et al.* Global formation of topological defects in the multiferroic hexagonal manganites. *Phys. Rev. X* **7**, 041014 (2017).

[17] Kosterlitz, J. M. & Thouless, D. J. Ordering, metastability and phase transitions in two-dimensional systems. *J. Phys. C: Solid State Phys.* **6**, 1181–1203 (1973).

[18] Sort, J. *et al.* Imprinting vortices into antiferromagnets. *Phys. Rev. Lett.* **97**, 067201 (2006).

[19] Wu, J. *et al.* Direct observation of imprinted antiferromagnetic vortex states in CoO/Fe/Ag(001) discs. *Nat. Phys.* **7**, 303–306 (2011).

[20] Wintz, S. *et al.* Topology and origin of effective spin meron pairs in ferromagnetic multilayer

elements. *Phys. Rev. Lett.* **110**, 177201 (2013).

[21] Shinjo, T., Okuno, T., Hassdorf, R., Shigeto, K. & Ono, T. Magnetic vortex core observation in circular dots of permalloy. *Science* **289**, 930–932 (2000).

[22] Senthil, T., Vishwanath, A., Balents, L., Sachdev, S. & Fisher, M. P. Deconfined quantum critical points. *Science* **303**, 1490–1494 (2004).

[23] Griffin, S. M. *et al.* Scaling behavior and beyond equilibrium in the hexagonal manganites. *Phys. Rev. X* **2**, 041022 (2012).

[24] Shimomura, N. *et al.* Morin transition temperature in (0001)-oriented α-Fe_2O_3 thin film and effect of Ir doping. *J. Appl. Phys.* **117**, 17C736 (2015).

[25] Yu, Y.-S., Jung, H., Lee, K.-S., Fischer, P. & Kim, S.-K. Memory-bit selection and recording by rotating fields in vortex-core cross-point architecture. *Appl. Phys. Lett.* **98**, 052507 (2011).

[26] Nakano, K. *et al.* All-electrical operation of magnetic vortex core memory cell. *Appl. Phys. Lett.* **99**, 262505 (2011).

[27] Parkin, S. S. P., Hayashi, M. & Thomas, L. Magnetic domain-wall racetrack memory. *Science* **320**, 190–194 (2008).

[28] Tomasello, R. *et al.* A strategy for the design of skyrmion racetrack memories. *Sci. Rep.* **4** (2014).

Methods

Sample Growth

α-Fe_2O_3 epitaxial thin films were prepared on c-Al_2O_3 single-crystal substrates by sputtering; c-Al_2O_3 single crystals were selected as substrates due to the moderate lattice mismatch, 5.3 %, and the identical space groups (R $\bar{3}c$). The (0001)-orientated films were grown 10 nm thick using on-axis RF magnetron sputtering at 500°C with an Ar:O_2 ratio of 3:2 and a chamber pressure of 400 mTorr. A 2-inch diameter stoichiometric α-Fe_2O_3 sputtering target (99% purity) was used at a sputtering power of 100 watts, yielding a deposition rate of 6.25 nm min^{-1}. The 1 nm, ferromagnetic Co overlayer was deposited, in the absence of a magnetic field, by DC magnetron sputtering at room temperature. The 1 nm Al layer was then deposited, by the same technique, to passivate the surface of the sample and prevent oxidation of the Co layer.

Structural Properties

The epitaxial nature of the film was confirmed using a Rigaku SmartLab diffractometer (Cu). The film was found to be majority phase α-Fe_2O_3 (with minor evidence, $\approx$ 1% by volume, of the oxygen deficient Fe_3O_4 phase). The measured c lattice parameter, 13.75 (2) Å, is in agreement with the bulk α-Fe_2O_3 value, indicating that the film is fully relaxed. The narrow rocking curve of the (0,0,6) reflection (FWHM = 0.47°- see Supplementary Figure 1c) additionally confirms the epitaxial nature of the film. The in-plane epitaxy of the film was investigated by ϕ scans of the {1,0,10} reflections of the α-Fe_2O_3 film and Al_2O_3 substrate

(Supplementary Figure 1b). The respective {1,0,10} reflections are coincident in direction for both α-Fe_2O_3 and Al_2O_3. The film thickness was confirmed to be approximately 10 nm by X-ray reflectivity.

MOKE magnetometry

Longitudinal Magneto-Optic Kerr effect magnetometry (L-MOKE) of the α-Fe_2O_3/Co confirmed that the Co layer was ferromagnetic, with a coercive field of 8 mT (Supplementary Figure 2). No appreciable Kerr rotation was observed for an isolated α-Fe_2O_3 film, confirming the signal arose from the Co layer and not the weak ferromagnetic moment of α-Fe_2O_3.

X-PEEM measurements and characterisation

The sample was mounted in a ultra high vacuum PhotoEmission Electron Microscopy (PEEM) chamber, where polarised x-rays are incident on the sample at a grazing angle of 16°. The x-ray beam is rastered such that a 20 µm is illuminated by the incident x-ray beam. Secondary electrons of any photoexcitation emitted from the sample surface are recorded using an electron microscope, yielding an optimal spatial resolution of $\sim$ 50 nm. Practically the resolution can be lower as a result of sample drift and non-optimal optical alignment. The sample could be rotated about its surface normal such that the incident x-ray direction could be altered. A field-of-view of 10 µm was used for all measurements which are stored in a 1024 $\times$ 1024 pixel grid; the width of each pixel being approximately 10 nm. Data reduction, distortion and drift corrections were performed using Igor Pro.
Several *in-situ* characterisation measurements were performed. Firstly, the total photoemission of a $\sim$ 20 µm diameter area was recorded as a function of energy for incident light of differing polarity (Supplementary Figure 3). The x-ray absorption spectra (XAS - the total photoemission is proportional to the number of photons absorbed per unit energy) about the Co-L_3 and Co-L_2 edges confirm that the layer was not oxidised (there is no visible crystal field splitting of the L_3 and L_2 edges).[29] The large dichroism under circular light additionally confirms that the layer was ferromagnetically ordered (Supplementary Figure 3a). The α-Fe_2O_3 layer was investigated by using linear horizontal and linear vertical polarised light (Supplementary Figure 3b). The structure of the XAS is consistent with Fe^{3+} in an octahedral environment, with a crystal field strength of 10Dq = 1.45eV, as opposed to it being either metallic or tetrahedrally coordinated.[30]

Co XMCD vector map construction

Magnetic vector maps of the ferromagnetic Co overlayer are constructed by imaging the x-ray circular magnetic asymmetry, δ, at two orthogonal incident x-ray directions and utilizing its angular dependence,

$$\delta \propto \mathbf{M} \cdot \hat{\mathbf{k}},$$

where $\mathbf{M}$ is the average magnetisation of the probed region and $\hat{\mathbf{k}}$ the incident x-ray direction.[31] Experimentally, δ is measured using incident light of both helicities (positive and negative circular) and two energies,

$$I_{pc} = \frac{I_{pc,E_1}}{I_{pc,E_2}} - 1,$$
$$I_{nc} = \frac{I_{nc,E_1}}{I_{nc,E_2}} - 1,$$
$$\delta = \frac{I_{pc} - I_{nc}}{I_{pc} + I_{nc}}.$$

In the case of Co, the two incident energies are the maximum of the L_3 edge, $E_1 = 777$ eV, and a (pre-edge) value, $E_2 = 770$ eV. By normalising the images recorded on the L_3 maximum (sensitive to the magnetic order) by an image recorded with a pre-edge energy we minimized spurious image contrast arising due to differences polarisation channels and/or small variations in the x-ray beam as a function of time.
By measuring the intensity of the XMCD at two orthogonal incident x-ray directions (Supplementary Figure 4), we can measure the local magnetisation to within a global scale factor,

$$\mathbf{M} \propto \delta_0 \hat{\mathbf{x}} + \delta_{\frac{\pi}{2}} \hat{\mathbf{y}},$$

where the orthogonal unit vectors $\hat{\mathbf{x}}$ and $\hat{\mathbf{y}}$ are defined by $\hat{\mathbf{k}}$ at 0 and $\frac{\pi}{2}$ radians respectively. Topological defects were identified in the Co vector map by calculating the winding number around a closed path (perimeter of a 5x5 pixel box) centred on each pixel. Regions with a calculated winding number of ± 1 were identified as vortices/anti-vortices respectively.

α-Fe_2O_3 XMLD vector map construction

Our vector map generation relies on the angular dependence of x-ray magnetic linear dichroism (XMLD). The angular dependence of the XMLD depends strongly on the relative orientation of the linear polarization, the spin direction, and the crystal axes.[32] Assuming (near) cubic symmetry for the lattice and with the surface normal a 3-fold axis, the angular dependence of the XMLD in the (0,0,1) plane due to the crystal field will vanish.
If α is the angle between the spin direction and the linear horizontal polarization in the (0,0,1) plane, then from the symmetry of the linear polarization it is clear that,

$$I_{LH}(\alpha) = I_C + I_M \cos(2\alpha),$$

where I_C is the constant part and I_M is the magnetization dependent part of the XAS. Neglecting the 16° grazing incidence angle of the beam, I_{LV} has the linear polarization along the normal and is independent of α. Taking the difference between I_{LH} and I_{LV} gives,

$$I_{XMLD}(\alpha) = I_{LH}(\alpha) - I_{LV} = I_{C'} + I_M \cos(2\alpha) = I_{C'} + I_M(2\cos(\alpha)^2 - 1),$$

XMLD maps are constructed by recording the photoemission with incident light of 709.1 eV and 708.4 eV (E_1, E_2) of both linear horizontal (LH) and linear vertical polarisations (LV). XMLD images are then constructed from a minimum of two images. Data presented in the main text were constructed from four images (two energies, two polarisations) where,

$$I_{LH} = \frac{I_{LH,E_1}}{I_{LH,E_2}} - 1,$$
$$I_{LV} = \frac{I_{LV,E_1}}{I_{LV,E_2}} - 1.$$

The asymmetry, δ - proportional to I_{XMLD}, is then calculated,

$$\delta = \frac{I_{LH} - I_{LV}}{I_{LH} + I_{LV}}.$$

The antiferromagnetic spin direction vector map is reconstructed by recording these images at multiple directions of the incident x-ray beam. For each pixel we fit the expected angular dependence of the XMLD signal (I_{XMLD}) to extract the average spin direction of the pixel (Supplementary Figure 5). Errors on the measured dichroism are counting errors on the raw images, appropriately propagated.

Data availability

The data used in this paper can be accessed at DOI: 10.5287/bodleian:g78B6Ry64.

[29] Okada, K. & Kotani, A. Complementary roles of Co 2p X-ray absorption and photoemission spectra in CoO. *J. Phys. Soc. Jpn.* **61**, 449–453 (1992).

[30] Van der Laan, G. & Kirkman, I. W. The 2p absorption spectra of 3d transition metal compounds in tetrahedral and octahedral symmetry. *J. Phys.: Condens. Matter* **4**, 4189 (1992).

[31] Stöhr, J. & Siegmann, H. C. *Magnetism: from fundamentals to nanoscale dynamics*, volume 152. Springer Science & Business Media (2007).

[32] Arenholz, E., van der Laan, G., Chopdekar, R. V. & Suzuki, Y. Anisotropic X-ray magnetic linear dichroism at the Fe $L_{2,3}$ edges in Fe_3O_4. *Phys. Rev. B* **74**, 094407 (2006).